$$p_1 = 0.868165 \times 10^{-3}, \quad p_2 = 0.36496 \times 10^{-2}$$

and the first arc time equal to 23.7 sec, the final arc equal to 49.8 sec, and a total time of 73.5 sec. The Hamiltonian can be shown to be equal to zero along the trajectory by using the forward and backward solutions of the adjoint variable.

Taking the limit as the lower control constraint is taken to zero, the phase portrait is derived and shown in Fig. 13 for the case with lower control constraint of 0°.

References

[1] Truxal, J. G., *Control System Synthesis*, McGraw-Hill, New York, 1955.

[2] Pontryagin, L. S. et al., *The Mathematical Theory of Optimal Processes*, Wiley, New York, 1962.

[3] Johnson, C. D., "Singular Solutions in Problems of Optimal Control," *Advances in Control Systems*, edited by C. T. Leondes, Academic Press, New York, 1965.

FEBRUARY 1971 J. AIRCRAFT VOL. 8, NO. 2

Optimum Horizontal Guidance Techniques for Aircraft

HEINZ ERZBERGER* AND HOMER Q. LEE*
NASA Ames Research Center, Moffett Field, Calif.

In the design of advanced flight control systems, consideration is currently being given to the problem of performing various terminal area maneuvers automatically. This paper discusses some problems of automatic guidance of an aircraft in the horizontal plane. The horizontal guidance tasks, which such a flight control system should be capable of performing, have been identified as being of three types: guiding the aircraft from any initial location and initial heading to a) any final location and heading; b) intercept and fly along a line of specified direction; and c) a final location with arbitrary final heading. Guidance problems, such as capturing an ILS beam at a specified point on the beam, intercepting a VOR radial, and point to point navigation, can be formulated in terms of these problems. The guidance laws given in this paper minimize the arc length of the trajectories to fly between initial and final conditions subject to a constraint on the turning radius of the aircraft. Application of the Minimum Principle to these problems has shown that the trajectories consist of a sequence of minimum radius turns and straight-line segments. At most, four partial turns may be required in problem a and two turns in problem b and c. A simple geometric technique is outlined for constructing the optimum trajectories graphically. The optimum control laws are derived for problems b and c.

Introduction

FLIGHT control systems for aircraft are rapidly evolving toward the automation of many traditional piloting functions. Increased automation in flight control systems has been made possible by the advent of flight worthy computers, and is found to be necessary for the safe and economical operation of such advanced aircraft as the SST and some V/STOL aircraft. A concept of automatic flight control which is now evolving aims at the automation of nearly all traditional piloting functions, leaving the flight crew to exercise chiefly managerial and supervisory control over the system.

Many diverse and complex research problems arise in the design of such a flight control system. The problem studied in this paper deals with the automatic guidance of the aircraft in the horizontal plane. The most often encountered problems in horizontal guidance, which in current terminal area operations are largely solved jointly by the pilot and the air traffic controller, can be classified into three types: a) flying from an initial point and heading to a specified final point and heading; b) flying from an initial point and heading to intercept, and then fly along a line of specified heading; and c) flying from an initial point and heading to a specified final point with arbitrary final heading.

The three problems previously defined have particular significance in terminal area guidance. Problems of type b occur when the aircraft is to capture an ILS beam or when it is to acquire and then fly along a particular VOR radial. If in addition the aircraft is to capture the beam or acquire the radial at a specified point, the guidance problem is of type a. In the ILS beam capture maneuver such a point might be the outer marker.

Many more complicated horizontal guidance problems can often be interpreted as a sequence of these three types of problems. For example, a holding pattern can be generated by flying in a specified sequence through a set of way points, where the guidance problem from one-way point to another is interpreted as a problem of type a or c, the choice depending on whether or not the heading of the aircraft when it arrives at the way points is specified or free. Similarly, guidance along entire flight profiles from takeoff to landing can be divided into a sequence of problems a, b, and c. The solution of these three guidance problems therefore assumes some importance in the development of an automatic guidance system and hence, is the subject of this paper.

In addition to horizontal guidance, vertical guidance and airspeed management must also be performed by the flight control system. However, except in special flight situations, horizontal guidance can be performed independent of vertical guidance and airspeed management, and this assumption will be used throughout this paper.

The three guidance problems defined here have the drawback of admitting an infinite number of flight trajectories for their solution. For example, in flying an aircraft from an initial position and heading to some specified final position and heading, a pilot may use a few steep turns and a number of straight-flight sections, or he may use several gently curved

Received December 10, 1969; revision received May 4, 1970.
* Research Scientist.

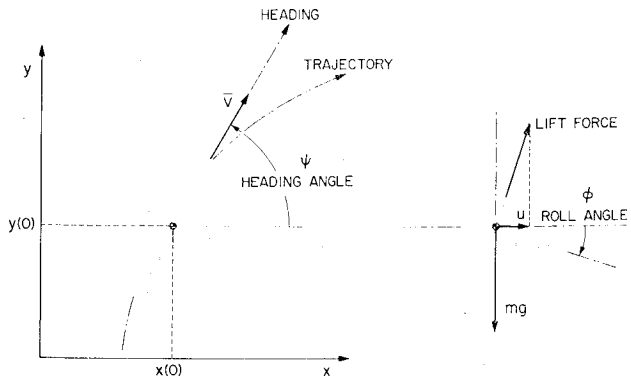

Fig. 1 Top and rear view of aircraft during a turn.

turns in addition to straight-flight sections, the exact maneuver depending on the problem as well as on the pilot. In developing a computer oriented synthesis procedure for the trajectories, it is necessary to specify a technique which generates efficient and predictable trajectories for all initial and final conditions. In this paper, the trajectories are calculated to minimize the arc length of the trajectories connecting initial and final conditions subject to a constraint on the minimum turning radius of the aircraft. The minimum turning radius is treated as a parameter and can be selected arbitrarily within the restriction that it be larger than the absolute minimum turning radius calculated in flight mechanics.[1] Considerations of passenger comfort would normally require the use of a minimum turning radius much larger than the absolute minimum because of the high-roll angles and the resulting high normal accelerations associated with flying the absolute minimum turning radius.

A general description of a concept for a highly automated flight control system was given by Petrie.[2] The problem of automatically guiding an airplane to capture an ILS beam in near minimum time was recently described by McKinnon.[3] This problem is similar to problem b defined earlier.

This paper is restricted to establishing the general characteristics and the theory for the calculation of the trajectories under the conditions previously given. The problem of flying along the generated trajectories by use of an autopilot and a navigation system is not considered.

Equations of Motion for Horizontal Guidance

A simplified set of equations is used here to describe the motion of the aircraft projected on the horizontal plane. It is assumed that the aircraft flies in a stationary air mass with small flight path angles and flight path angle rates, such that the lift is essentially equal to the aircraft weight. Turns achieved by banking the aircraft are assumed to be coordinated with the yaw rate so as to maintain zero sideslip. Furthermore, the roll time constant is neglected and thrust is set equal to drag. Under these conditions, the motion of the aircraft in the horizontal plane is described by the following set of equations:

$$dx/dt = v_x \tag{1}$$

$$dy/dt = v_y \tag{2}$$

$$dv_x/dt = u/m \sin\psi \tag{3}$$

$$dv_y/dt = -u/m \cos\psi \tag{4}$$

In these equations, m is the aircraft mass ψ is the heading angle defined by $\psi = \tan^{-1} v_y/v_x$, and u is the horizontal force, which is related to the bank angle ϕ by $u = w \tan\phi$, where w is the aircraft weight. Either of the quantities ϕ or u may be considered the control variable in this problem. By convention, clockwise rotation or, equivalently, right-wing down defines the positive bank angle. Further details on aircraft equations of motion applicable to this problem can be found in Ref. 1. Figure 1 helps to visualize the geometric relationships of some variables defined here.

The problem of minimizing the arc length of trajectories with a constraint on the minimum turning radius can be converted into the problem of minimizing the time to fly between specified initial and final conditions. It is assumed that the constraint is independent of the horizontal velocity. Trajectories minimizing the arc length will be identical to trajectories minimizing the transition time if the latter are computed subject to the conditions that the magnitude v of the horizontal velocity, defined as $v = (v_x^2 + v_y^2)^{1/2}$, is constant during the motion, and that the minimum turning radius constraint is converted into an equivalent maximum bank-angle constraint. At a constant horizontal velocity, the relationships between minimum turning radius $R_{\min}$ maximum bank angle $\phi_{\max}$, and maximum force $u_{\max}$ are as follows:

$$R_{\min} = v^2/(g \tan|\phi_{\max}|) \tag{5}$$

$$u_{\max} = w \tan|\phi_{\max}| \tag{6}$$

where g denotes the acceleration of gravity.

In the subsequent analysis, the equivalent minimum time problem is discussed. It can be shown that the quantity v is, as required, a constant of the motion in Eqs. (1–4).

The equations of motion can be normalized if the following transformation of variables is introduced: $x = \alpha\hat{x}$, $y = \alpha\hat{y}$, $v_x = \beta\hat{v}_x$, $v_y = \beta\hat{v}_y$, and $t = \delta\hat{t}$. If the constants of α, β, δ are chosen as $\alpha = vm/u_{\max}$, $\beta = v$, $\delta = m/u_{\max}$, the equations in the transformed variables can be written as

$$d\hat{x}/d\hat{t} = \hat{v}_x \tag{7}$$

$$d\hat{y}/d\hat{t} = \hat{v}_y \tag{8}$$

$$d\hat{v}_x/d\hat{t} = u/u_{\max}\hat{v}_y \tag{9}$$

$$d\hat{v}_y/d\hat{t} = -u/u_{\max}\hat{v}_x \tag{10}$$

with $\hat{v}_x^2 + \hat{v}_y^2 = 1$. It follows that no loss in generality results if in the analysis the constants m, v, and $u_{\max}$ are chosen to be unity. Throughout the remainder of the paper this choice of the constants is tacitly assumed. Furthermore, the hat notation for the transformed variables is dropped.

Formulation of Optimal Guidance Problem

With the transition time as the performance index and the equations of motion derived earlier as the state equations, the three horizontal guidance problems can be formulated as problems in optimal control. Application of the Minimum Principle to these problems yields the following set of relations:[4]

$$\text{Hamiltonian: } H = \min_u [1 + \lambda_x v_x + \lambda_y v_y + u(\lambda_{v_x} v_y - \lambda_{v_y} v_x)] \tag{11}$$

$$H(t) = 0 \text{ for all } t \tag{12}$$

System equations: (7–10)

$$\text{Control constraint: } |u| \leq 1 \tag{13}$$

$$\text{Adjoint equations: } d\lambda_x/dt = 0 \tag{14}$$

$$d\lambda_y/dt = 0 \tag{15}$$

$$d\lambda_{v_x}/dt = u\lambda_{v_y} - \lambda_x \tag{16}$$

$$d\lambda_{v_y}/dt = -u\lambda_{v_x} - \lambda_y \tag{17}$$

Initial conditions for system equations are, $x(0)$, $y(0)$, $v_x(0)$, $v_y(0)$ where $v_x^2(0) + v_y^2(0) = 1$.

Initial conditions for adjoint equations to be determined so as to satisfy final conditions given below.

Final time: free, denoted by T.

The final conditions for the system and adjoint equations differ for the three problems and, for the case of the adjoint equations, are determined by the transversality conditions.[4] In addition, the final conditions for the system equations are chosen, without loss of generality, in a particular manner to simplify the analysis.

Final conditions:

Problem a) $x(T) = 0; y(T) = 0; v_x(T) = 1; v_y(T) = 0$
$\lambda_x(T), \lambda_y(T), \lambda_{v_x}(T), \lambda_{v_y}(T)$ free

Problem b) $x(T)$ free; $y(T) = 0; v_x(T) = 1; v_y(T) = 0$
$\lambda_x(T) = 0; \lambda_y(T), \lambda_{v_x}(T), \lambda_{v_y}(T)$ free

Problem c) $x(T) = 0; y(T) = 0; v_x(T), v_y(T)$ free; $\lambda_x(T)$,
$\lambda_y(T)$ free; $\lambda_{v_x}(T) = 0, \lambda_{v_y}(T) = 0$

The solution of the optimal guidance problem thus reduces to finding a solution to the well known two-point boundary-value problem of selecting the initial conditions of the adjoint equations, so as to generate a control time history that satisfies the necessary conditions of the Minimum Principle and transfers the initial state to the desired final state. This problem is examined in subsequent sections.

Minimization of Hamiltonian and the Existence of Singular Controls

In application of the Minimum Principle, the minimum condition in the Hamiltonian Eq. (11), is used to determine the optimum control, denoted by u^*, as a function of the state and the adjoint variables for all values of these variables that yield a unique minimizing control. A time optimum control problem is called "normal" if a unique minimizing control exists for all except isolated instants of time. Reference 4 may be consulted for a discussion of normality. For the case at hand, minimization over u in Eq. (11) obtains

$$u^* = -\text{sgn}(S), S \neq 0 \tag{18}$$

where

$$S \equiv \lambda_{v_x} v_y - \lambda_{v_y} v_x$$

which is the well known bang-bang control law. As might be surmised from physical considerations, this problem is not normal, suggesting the possible existence of singular optimum controls which may occur whenever S is identically zero for a nonzero time interval. The method which can be used for computing those values of the control, which are candidates for singular optimum controls, is the one described in Ref. 5. Briefly stated, this method consists of determining the control u, called the singular control, as a function of the state and adjoint variables, such that use of u will keep S identically zero within some nonzero time interval if it is zero at the beginning of the interval.

Application of this method shows that $u = 0$ is the only candidate for a singular control, and that the condition for getting onto a singular trajectory is given by the simultaneous solution of the following equations:

$$\lambda_x^2 + \lambda_y^2 = 1 \tag{19}$$

$$\lambda_x = -v_x \tag{20}$$

$$\lambda_y = -v_y \tag{21}$$

$$\lambda_{v_x} v_y - \lambda_{v_y} v_x = 0 \tag{22}$$

Physical interpretation of the preceding equations and derivations yields some important properties of the optimum trajectories. Thus, it follows from Eq. (18), and some easily established properties of the system Eqs. (7–10), that non-

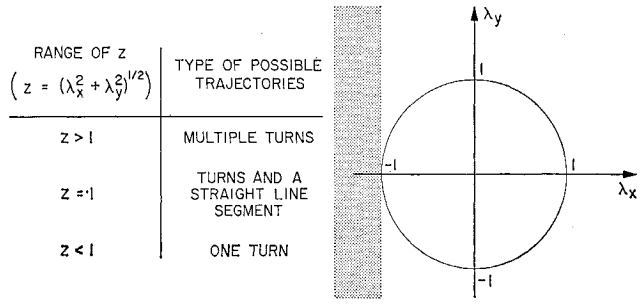

Fig. 2 Restrictions on the choice of λ_x and λ_y; for $v_x(0) = 1$, points in the shaded region are excluded.

singular intervals of optimum trajectories consist of turns with maximum bank angle and hence, minimum turning radius, whereas singular intervals of optimum trajectories consist of straight-line flight. Furthermore, in each optimum trajectory there is only one direction of flight or, equivalently, heading angle, along which the trajectory can be singular. This property follows from Eqs. (20) and (21) and the fact that λ_x and λ_y are constants for any given optimum trajectory. Finally, once a trajectory has entered a singular interval, it will remain singular as long as u is held at zero, implying that the singular trajectories, interpreted as straight lines in the horizontal plane, need not be bounded. The length of the singular interval must therefore be determined from the requirement that the states achieve specified final conditions. In subsequent discussions, a singular interval will be referred to by the geometrically more descriptive name of straight-line segment.

Properties of the Optimum Trajectories

Additional properties of the optimum trajectories can be obtained by expressing the switching function S as a function of time and initial conditions of the state and adjoint variables. As the initial conditions on the adjoint variables in $S(t)$ are varied through their permissible range of values, all possible optimum control time histories are generated by the expression $u^* = -\text{sgn}S$. A list of possible optimum trajectories distinguishable on the basis of the shape of the curves they generate in state space can therefore be derived from this study of S.

In order to solve for S, it is first necessary to obtain solutions to the state and adjoint equations. These solutions can be obtained by assuming that u is piecewise constant, since it was previously shown that u can take on only the three values -1, 0, and 1. Under these conditions, Eqs. (7–10) and (14–17) become linear and can be solved by known techniques. The solutions to these equations are then substituted into the expression for S and also into Eq. (12). After some algebraic simplifications, which involve the use of simple trigonometric identities and the relation obtained for $H(t)$, the switching function S can be written as follows in a time interval during which S does not change sign:†

$$S = -1/u^*\{1 + z\cos[u^*t + \zeta - \psi(0)]\} \tag{23}$$

where ζ and z are defined by $\zeta \equiv \tan^{-1}\lambda_y/\lambda_x$, $z \equiv (\lambda_x^2 + \lambda_y^2)^{1/2}$, and u^* is either -1 or 1. The quantity $\hat{S}$ defined by

$$\hat{S} = 1 + z\cos[u^*t + \zeta - \psi(0)] \tag{24}$$

must be greater than zero in each time interval in which S is not zero. The effect of this restriction on the sign of $\hat{S}$ is to limit the freedom of choosing λ_x and λ_y, with the range of permissible values of these variables depending on the

† Because of the normalization, all variables can be taken as dimensionless quantities.

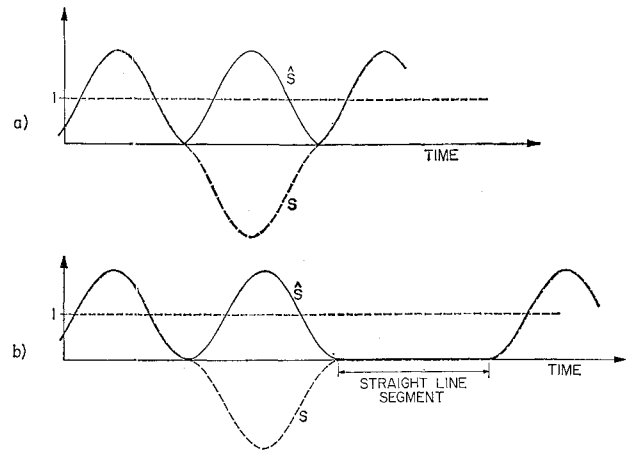

Fig. 3 Example time histories of the functions S and $\hat{S}$ for two values of z: a) $z > 1$ and b) $z = 1$.

initial heading $\psi(0)$. The range of permissible values is a half plane which includes the circle $z = 1$ and whose boundary is the line which touches the circle $z = 1$ at a point on the circle defined by $\zeta = \psi(0) + \pi$. Figure 2 illustrates the restriction in the choice of λ_x and λ_y for $v_x(0) = 1$.

It is seen from the expression for S that no sign changes in S and hence, no switchings in the control u^* can occur for λ_x, λ_y lying in the interior of the circle $z = 1$. Switchings in the sign of the control can occur only for $z \geq 1$. The condition $z = 1$ makes possible the occurrence of a straight-line segment. This fact is obtained by using Eq. (23) to show that $z = 1$ implies $S = 0$. The relationship between z and the possible control sequence in a trajectory is also given in Fig. 2.

Although the solutions for S and $\hat{S}$ given previously are restricted to time intervals during which S does not change sign and u^* is constant, the continuity with respect to time of $\dot{S}$ can be used to generate time histories of S and $\hat{S}$ across instants of sign change of S. Continuity of $\dot{S}$ follows from Eq. (19). Representative time histories of S and $\hat{S}$ are shown in Fig. 3a for a value of z slightly larger than 1 and in Fig. 3b for $z = 1$.

It can be seen by interpreting Eq. (23) and Fig. 3b that the most general form of a trajectory containing a straight-line segment consists of a turn of less than 2π radians followed by a straight line followed by another turn of less than 2π radians. The angles in the turns and their direction as well as the length of the straight-line segment must in each case be selected to satisfy the initial and final conditions of the problem.

Since additional properties of the optimum trajectories depend on the nature of the end conditions of the state and adjoint variables, each of the three problems defined earlier is now examined separately. In problem a the end condition of the adjoint variables are free, implying that all combinations of λ_x and λ_y falling within the restrictions illustrated in Fig. 2 can occur. Only nonsingular trajectories are examined here since the singular case was covered in the previous paragraph. With these facts in mind, Eq. (23) can be used to calculate the range of angles in the turn between the first and the second switching time as a function of the angle in the turn from the initial time to the first switching time. The procedure for calculating this relationship is to let z and ζ vary over all permissible values and to observe how such variations can affect the time between switchings. The use of Figs. 2 and 3 helps to simplify this task. It is seen that in any optimum trajectory containing three turns or, equivalently, two switching times, the middle turn must contain more than π radians. Furthermore, it can be seen from Fig. 3a that the time interval between the first and the second switching time equals the time interval between the second and the third switching time. Therefore, it follows that in a trajectory containing four turns, the two middle turns must, in addition to containing more than π radians, also contain equal number of radians. Finally, no optimum trajectory can contain more than three switching times or, equivalently, four turns.‡ This upper limit on the number of switchings can be established by considering an arbitrary trajectory containing four switchings and by showing that such a trajectory can always be reduced in length. Thus, in the example trajectory with four switchings shown in Fig. 4, a tangent line from the second to the fourth partial circle, which can always be drawn because each of these partial circles must contain more than π radians, eliminates the third partial circle entirely, and therefore yields a shorter trajectory.

Problems b and c are discussed next, but in less detail since they can be solved by the same techniques as developed in the solution of problem a. In problem b, the condition $\lambda_x = 1$ implies that the heading angle of a straight-line segment, if it occurs, must be perpendicular to the final heading. Furthermore, it can be shown that optimum trajectories with no straight-line segments consist of no more than two turns, of which the final turn, if it occurs, must contain an angle in the range between zero and $\pi/2$ or π and $3\pi/2$ radians. Finally, optimum trajectories for problem c consist of either a turn followed by a straight line or two turns of which the final turn, if it occurs, must contain an angle larger than π radians.

A summary of all possible optimum trajectories for the three problems is presented in Table 1. This table contains all optimum trajectories that can be distinguished on the basis of shape but does not include the mirror images of these trajectories which can also be optimum. The orientation of the patterns was chosen for convenience of illustration, and no special significance should be attached to it. When applicable, conditions for optimality are indicated next to the trajectory to which they apply.

A procedure for geometrically constructing optimum trajectories for problem a is described in the Appendix.

Example for Problem a

As an example, assume the initial heading equals the final heading, and the line connecting the initial point P_o with the final point P_f is perpendicular to the direction of the final heading. Optimum trajectories are to be determined for all values of the distance P_oP_f. In order of increasing distance, the optimum trajectories consist of 1) two arcs and their common external tangent (pattern a, Fig. 5a), 2) three arcs (pattern b, Fig. 5a), 3) two arcs (pattern c, Fig. 5a), and 4) two arcs and their common internal tangent (pattern d, Fig. 5a) Figure 5b exhibits the relation between the total length or, equivalently, the transition time, of the optimum trajectories and the parameter P_oP_f. Change

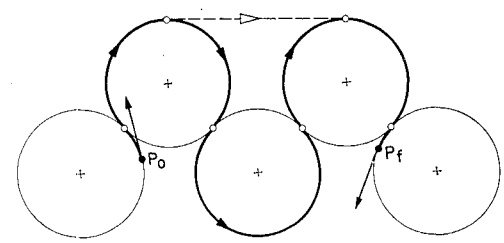

Fig. 4 Reducing the length of a trajectory containing five-circular arcs.

‡ It is not ruled out that this limit can be reduced to two switchings or, equivalently, three turns, although a proof of it is lacking.

in pattern occurs where the distance is equal to 2.97 and 4, as indicated in the figure.

Control Law for Problem b

By using the properties of the optimum trajectories for this problem as enumerated in Table 1, an explicit description of the optimum control law can be developed. This control law is most easily expressed in terms of the parameters d and ψ, which are, respectively, the perpendicular distance of the aircraft's current position from the final line and the current heading angle ψ of the aircraft measured with respect to the direction of the final line. Positive distances are associated with those aircraft positions lying to the right of the final line when facing in the direction of the line's heading. Positive heading angles are defined in the conventional manner.

Figure 6 illustrates the control law in this d-ψ plane. The plane has been divided into three regions labeled turn left, turn right, and fly straight. The label of a region determines the control to be used for any parameter pair d and ψ falling in that region. The regions labeled turn left and turn right are bounded by sections of straight lines and portions of sine functions, whereas the region labeled fly straight consists of two-half lines that also form the trajectories for this choice of control. Trajectories generated by turns are parameterized in this plane by the equations

$$d_r(\psi) = d_o + \cos\psi_o - \cos\psi \text{ (right turn)}$$

$$d_l(\psi) = d_o - \cos\psi_o + \cos\psi \text{ (left turn)}$$

where d_o and ψ_o are the initial values of the parameters d and ψ. The final turns onto the line and straight-line flight are indicated in the figure by solid lines, with arrows giving the direction of motion along the lines. Except for the two segments of the final turns lying in the forbidden

Table 1 Summary of shapes of possible optimum trajectories

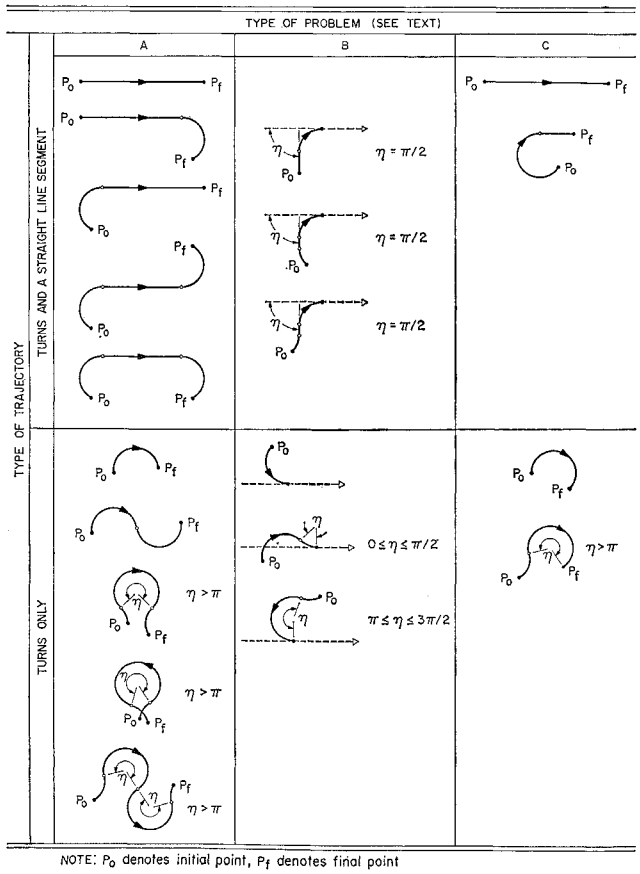

NOTE: P_o denotes initial point, P_f denotes final point

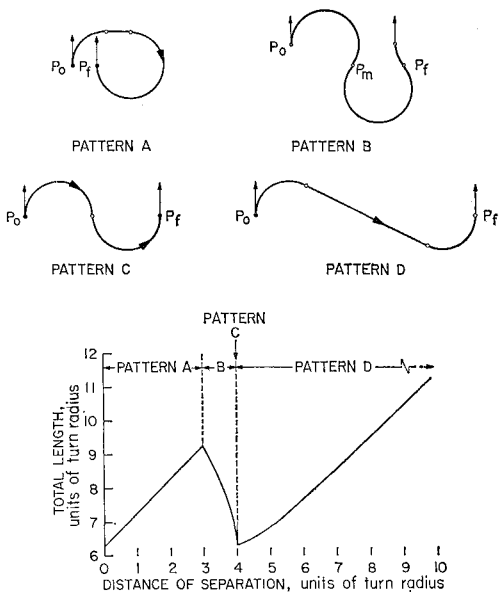

Fig. 5 The four possible patterns of optimum trajectories as a function of P_oP_f; example for problem a.

range of angles between $\pi/2$ and π, and $-\pi/2$ and $-\pi$, these lines coincide with the switching points for the control, and therefore also form a part of the boundary between the regions. The shading of these regions near the boundary formed by these lines has been exaggerated to give an indication into which region the line itself belongs. The part of the boundary not formed by these lines may be considered in either region.

The initial turns of some example trajectories are indicated in Fig. 6 by dashed lines.

Control Law for Problem c

Here, two circles and a line (drawn broken in Fig. 7a) divide the horizontal plane into four regions which are labeled as shown in Fig. 7a. The circles and the line pass through the initial point P_o and are tangent at this point to the line of initial direction indicated by the vector $\hat{n}_o$. An optimum trajectory for a given final point is obtained by performing the geometric construction indicated by the label of the region to which the point belongs. Example trajectories for a number of final points have been drawn in Fig. 7b.

Concluding Remarks

Trajectories minimizing the arc length subject to a constraint on the minimum turning radius have been computed

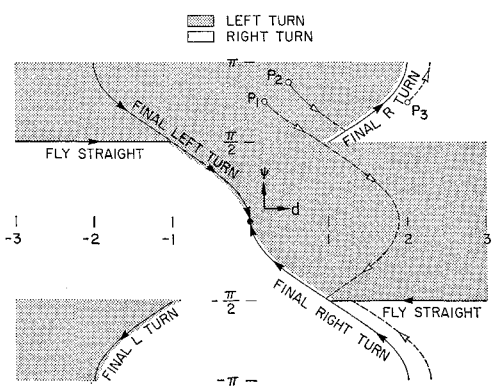

Fig. 6 Control law for problem b.

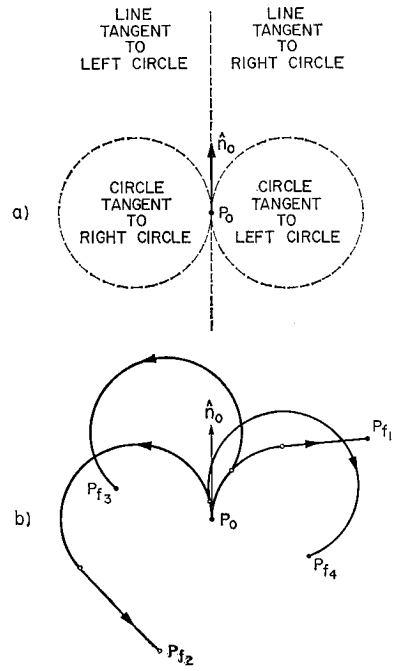

Fig. 7 Control law for problem c with example trajectories.

for three common maneuvering problems occurring in the terminal area. Optimum trajectories are found to consist of connected segments of straight lines and minimum radius turns. The trajectories are therefore parameterized by the turning radius, which may be assigned any value equal to or larger than the absolute minimum turning radius of the aircraft as computed in flight mechanics. Although only trigonometric equations would have to be solved to compute the trajectories, some simplification in the trajectories of problem a may be desirable, both from the standpoint of simplifying the computations as well as for reasons of operational acceptability of the trajectories. These simplifications are most likely to take the form of restricting the trajectories to consist of no more than two turns and one straight-line segment.

Appendix: Geometric Construction of Optimum Trajectories for Problem a

The special properties of the optimum trajectories summarized in Table 1 can be used to derive a set of trigonometric equations for the solution of the trajectories. Since a considerable number of equations are involved, they are not given here. Instead, a geometric construction procedure is described which is helpful in deriving the equations and in synthesizing switching logic.

Although the conditions of optimality help to determine the class of trajectories that can be optimum, they are in this problem not sufficient by themselves to yield a unique optimum trajectory for every possible combination of initial and final conditions. A geometric construction procedure must therefore generate all trajectories for arbitrary initial and final conditions that can satisfy the necessary conditions of the Minimum Principle. Each such trajectory will be called a feasible optimum trajectory. After all feasible optimum trajectories have been constructed, the globally optimum trajectory is found by choosing that feasible trajectory having the shortest transition time or, what is equivalent, the shortest arc length. Details of the construction technique are given here for problem a.

Denote by P_o and P_f the initial and final point and by ψ_o and ψ_f the initial and final heading, respectively. Determine the distance between P_o and P_f and mark these points on a sheet of paper, using the minimum turning radius computed from Eq. (5) as the unit of distance. Draw unit vectors $\hat{n}_o$ and $\hat{n}_f$ having direction ψ_o and ψ_f and emanating from P_o and P_f, respectively.

If $\hat{n}_o$, $\hat{n}_f$ and the directed line $\mathbf{P}_o\mathbf{P}_f$ are collinear and confluent, then the optimum trajectory is $\mathbf{P}_o\mathbf{P}_f$. Otherwise, draw lines containing $\hat{n}_o$ and $\hat{n}_f$ and draw two unity circles C_o, C'_o tangent to $\hat{n}_o$ at P_o and two unity circles C_f, C_f' tangent to $\hat{n}_f$ at P_f. Mark directions of travel on these lines so that these circles and lines are confluent with their respective vectors $\hat{n}_o$ and $\hat{n}_f$, as in Fig. 8a. The circles associated with P_o will be referred to as the initial circles, and those with P_f as the final circles and the lines containing P_o and P_f will be referred to as the initial and the final lines, respectively. If an initial and a final circle coincide and if the circles are confluent, then the optimum trajectory is a circular arc. If the initial circle is tangent to the final line and if the directed line from the point of contact with the circle to P_f is confluent with $\hat{n}_f$, then the trajectory consisting of one-circular arc and a line segment is a feasible optimum trajectory. Similarly, if a final circle is tangent to and confluent with the initial line, then the trajectory consisting of one-line segment and a circular arc is a feasible optimum trajectory. If an initial circle is tangent to a final circle such that their arcs are confluent, then the path traversed by the two arcs is a feasible optimum trajectory. Next, draw straight lines which are tangent to an initial and final circle, so that a confluent path is formed. In Fig. 8a only three tangents form confluent paths, although in general there may be as many as four. If the distance between P_o and P_f is greater than four radii, then the shortest feasible trajectory so far constructed is the optimum trajectory. Otherwise, it may not be optimum and must be compared with trajectories consisting of three and four-circular arcs.

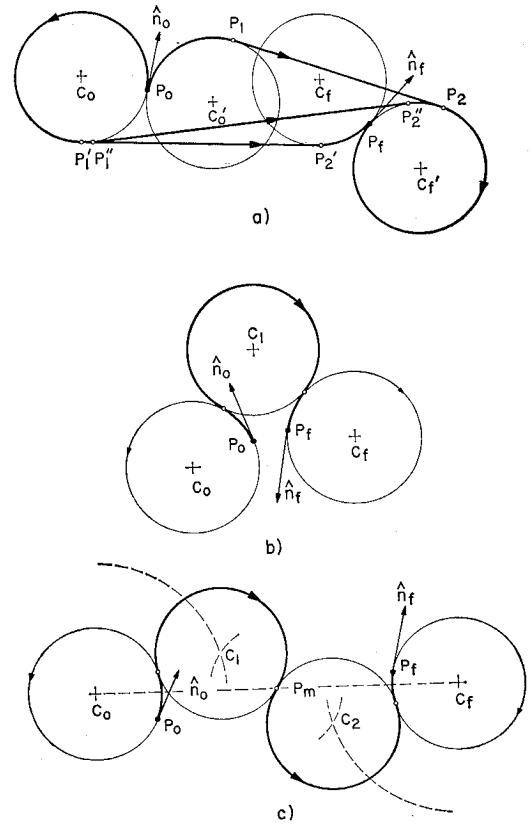

Fig. 8 Geometric construction of feasible optimum trajectories for problem a.

To synthesize the three-arc trajectory, draw a unity circle C_1 tangent to both C_o and C_f as in Fig. 8b. The center of C_1 is the intersection of two arcs which are two radii from C_o and C_f, respectively. By using different combinations of initial and final circles in this construction, up to eight such centers can be found. At most, two of these can be used to draw circles that form confluent three-arc trajectories and that contain angles of more than π radians. The shortest of these two is another feasible optimum trajectory.

To construct the four-arc trajectory, denote by P_m the midpoint of the line connecting the center of the circles C_o and C_f. Draw a unity circle C_1 tangent to C_o with center at the intersection of two arcs, the first arc being two radii from C_o and the second arc one radius from P_m, as illustrated in Fig. 8c. Similarly, draw a second circle C_2 tangent to both the final circle C_f and the circle C_1. This procedure guarantees that the two-interior arcs of the four-arc trajectory are of equal length. At most, two four-arc trajectories with interior arcs containing angles of more than π radians can be drawn by using different combinations of initial and final circles.

This concludes the construction of all feasible optimum trajectories. The globally optimum trajectory can now be determined by comparing the length of all feasible optimum trajectories, and choosing the one with the shortest arc length.

References

[1] Miele, A., "Theory of Flight Paths," *Flight Mechanics*, Vol. 1, Addison-Wesley, Reading, Mass., 1962, Chaps. 4 and 9.

[2] Petrie, D. M., "Automatic Flight Management of Future High-Performance Aircraft," *Journal of Aircraft*, Vol. 5, No. 4, July–Aug. 1968, pp. 335–343.

[3] MacKinnon, D., "Quasi-Optimization of a Localizer Acquisition System," *Proceedings of the 1969 Joint Automatic Control Conference*, American Institute of Chemical Engineers, 1969, pp. 822–830.

[4] Athans, M. and Falb, P. L., *Optimal Control*, McGraw Hill, New York, 1966, Chaps. 5 and 6.

[5] Johnson, C. D., "Singular Solutions in Problems of Optimal Control," in *Advances in Control Systems*, Vol. 2, edited by C. T. Leondes, Academic Press, N. Y., 1965, pp. 209–267.

FEBRUARY 1971 J. AIRCRAFT VOL. 8, NO. 2

Boundary-Layer Discontinuity on a Helicopter Rotor Blade in Hovering

HENRY R. VELKOFF,* DWIGHT A. BLASER,† AND KENNETH M. JONES‡

The Ohio State University, Columbus, Ohio

An experimental study was conducted using flow visualization techniques to investigate the nature of the boundary layer on a model helicopter rotor. Hovering and forward flight data were obtained; however, efforts were concentrated on hovering when unanticipated boundary-layer behavior was revealed. The primary flow visualization technique involved the use of ammonia injected into the boundary layer at the leading edge. The blade surface was chemically coated, and as the ammonia moved with the local airflow, it formed a trace on the surface indicative of the boundary-layer flow. The hovering traces initially moved chordwise along the surface, and then abruptly turned outward. A short distance later, the traces moved inward and then continued aft along the blade in a somewhat diffuse pattern. Similar traces were found over wide ranges of pitch angles and rotor speeds. It is hypothesized that a standing laminar separation bubble exists on the blade surface aft of the peak pressure position. No indication of any separation bubbles could be found on the forward flight traces.

Nomenclature

c = blade chord length
L_1 = separation point
L_2 = reattachment point
P = pressure coefficient
ΔP = differential pressure
q = dynamic pressure, $\rho V^2/2$
r = radius to local blade section
R = blade radius
s_1 = stagnation point preceding the separation bubble
s_2 = stagnation point following the separation bubble
V = flight speed
V_r = resultant potential flow velocity at radius r
x = distance along midchord measured from the blade leading edge
θ = blade pitch angle
μ = advance ratio
ψ = azimuth angle
Ω = rotational speed of rotor

Presented as Paper 69-197 at the AIAA/AHS VTOL Research Design, and Operations Meeting, Atlanta, Ga., February 17–19, 1969; submitted January 26, 1970; revision received June 17, 1970. This work was sponsored under a contract with the U.S. Army Aviation Materiel Laboratories, "AVLABS" Fort Eustis, Va.

* Professor of Mechanical Engineering.

† Graduate student.

‡ Graduate student; now Associate Research Engineer, SST Division, The Boeing Company, Seattle, Wash.

Introduction

A FUNDAMENTAL limitation on the performance and utility of the helicopter is related to the onset of "stall" on the retreating blades. This stall limits the performance of the helicopter because of increased power requirements, increased aircraft roughness, vibration, and control loads. Blade stall, however, depends upon the nature of the boundary layer which exists on an airfoil. Relatively little information on the nature of the boundary layers on rotor blades has existed until quite recently.[1–4] The complexity of the rotor blade motion, the flowfield, and the fluid mechanic equations involved have tended to discourage research into the nature of the rotor blade boundary layers. It was the purpose of